crystals

MDPI

*Article*

# Nematic Phases in Photo-Responsive Hydrogen-Bonded Liquid Crystalline Dimers

**Christian Anders, Muhammad Abu Bakar, Tejal Nirgude and Mohamed Alaasar ***

Institute of Chemistry, Martin Luther University Halle-Wittenberg, 06120 Halle Saale, Germany; christian.anders@chemie.uni-halle.de (C.A.); muhammad.abu-bakar@chemie.uni-halle.de (M.A.B.); tejal.nirgude@student.uni-halle.de (T.N.)

* Correspondence: mohamed.alaasar@chemie.uni-halle.de

**Abstract:** We report on the preparation and characterization of a new family of hydrogen-bonded nematogenic liquid crystalline dimers. The dimers are supramolecular complexes that consist of a benzoic acid derivative, acting as the proton donor, featuring a spacer with seven methylene groups and a terminal decyloxy chain, paired with an azopyridine derivative as the proton acceptor. The latter was either fluorinated or nonfluorinated with variable alkoxy chain length. The formation of a hydrogen bond between the individual components was confirmed using FTIR and $^{1}$H NMR spectroscopy. All supramolecules were investigated for their liquid crystalline behaviour via a polarized optical microscope (POM) and differential scanning calorimetry (DSC). All materials exhibit enantiotropic nematic phases as confirmed by X-ray diffraction (XRD) and POM investigations. The nematic phase range depends strongly on the degree and position of fluorine atoms. Additionally, the supramolecules demonstrated a rapid and reversible transition between the liquid crystal phase and the isotropic liquid state because of *trans-cis* photoisomerization upon light irradiation. Therefore, this study presents a straightforward approach to design photo-responsive nematic materials, which could be of interest for nonlinear optics applications.

**Keywords:** azopyridine; hydrogen bonding; fluorine; nematic phase; liquid crystals



Academic Editor: Benoit Heinrich

Received: 27 May 2025
Revised: 14 June 2025
Accepted: 16 June 2025
Published: 18 June 2025

**Citation:** Anders, C.; Abu Bakar, M.; Nirgude, T.; Alaasar, M. Nematic Phases in Photo-Responsive Hydrogen-Bonded Liquid Crystalline Dimers. *Crystals* **2025**, *15*, 576. https://doi.org/10.3390/cryst15060576



## 1. Introduction

The demand for advanced liquid crystalline (LC) materials with enhanced physical properties continues to grow, driven by the ever-expanding market for liquid crystal display (LCD) technologies in laptops, TVs, and other modern devices. While low-melting-point nematogenic and chiral smectic LCs dominate current applications, there is a pressing need for innovative materials that offer improved functionality and responsiveness [1,2]. Among the most promising strategies for designing such materials is the use of noncovalent interactions, particularly hydrogen bonding, to obtain ordered and complex supramolecular architectures [3]. Hydrogen bonding, especially between pyridine and benzoic acid derivatives, has proven to be a powerful tool for inducing nematic, smectic, and columnar mesophases [4–10]. It was also employed to induce more exotic phases, such as the twist-bend ($N_{TB}$) phase in LC dimers and mixtures of achiral components [11–13] and the recently discovered ferroelectric nematic phase ($N_F$) [14]. Beyond phase induction, hydrogen bonding has also been employed to induce chirality in isotropic liquids and stabilize bicontinuous cubic phases, highlighting its versatility in LC design [3,15–17].

Liquid crystal dimers, which consist of two mesogenic units connected by a flexible spacer, represent a unique class of materials whose properties often differ significantly

from those of their individual components. These dimers, whether symmetric or nonsymmetric, have served as a rich source for discovering new LC phases and understanding structure–property relationships [18–20]. When combined with photo-responsive units, such as azobenzene or azopyridine derivatives, LC dimers can exhibit light-driven behaviour, making them ideal candidates for applications in photonics, optoelectronics, and beyond [21–26]. Azopyridine derivatives offer a dual advantage: they retain the photo-responsive nature of azobenzenes while enabling self-assembly through intermolecular interactions, such as hydrogen bonding [9,14–16,27–29]. This combination makes them highly attractive for designing light-addressable materials with applications in molecular switches, photo-oscillators, and optogenetics [30–33].

Aromatic core fluorination is known as a successful tool to modify the mesophase behaviour of liquid crystalline materials due to its greater polarity and larger size compared to hydrogen [34]. Therefore, it has been used for different types of LCs such as rod-like molecules [35,36], discotics [37], and bent-core ones [38]. Fluorine's electronegativity and minimal steric effects promote polar behaviour, where the properties are strongly affected by the number and position of fluorine atoms [35,39]. Therefore, it was recently used to induce interesting polar phases in simple rod-like molecules [40,41].

In this study, we explore the design and characterization of a new family of hydrogen-bonded supramolecular photo-responsive liquid crystalline dimers (Scheme 1). The supramolecules are constructed by hydrogen bond formation between a benzoic acid derivative (**B**) with an aliphatic spacer with seven methylene groups as a proton donor and two different types of azopyridine derivatives (**A*n***  and **AF3*n***) as proton acceptors. This results in two groups of supramolecules, either without fluorine substitution (**A*n*/B**) or with an ortho F atom next to the terminal alkoxy chain at the azopyridine side (**AF$_3$*n*/B**). To investigate the effect of the position and degree of fluorination, two additional selected examples were constructed (**AF$_2$8/B** and **AF$_{23}$8/B**). Both have an octyloxy chain at the azopyridine component, but the former has an F atom at the meta position (**AF$_2$8/B**), while the latter has two F atoms at ortho and meta positions (**AF$_{23}$8/B**). This allows us to investigate the role of aromatic core fluorination on mesophase stability in the new supramolecular dimers. The photo-responsive behaviour of these materials, coupled with their self-assembly capabilities, opens new pathways for developing functional LC systems, which could be of interest for optical storage and adaptive photonic device applications.

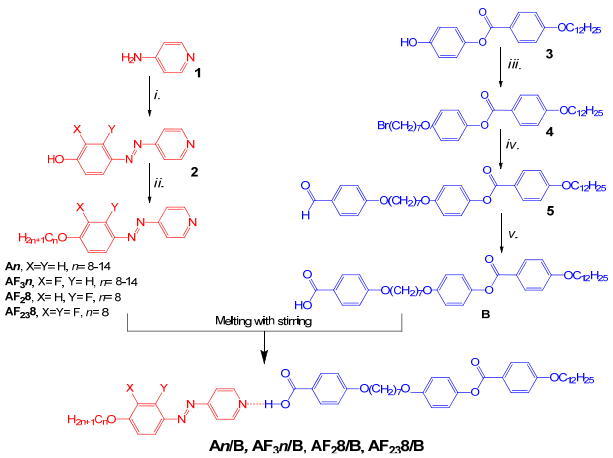


**Scheme 1.** Synthesis of hydrogen-bonded supramolecules **A*n*/B**, **AF$_3$*n*/B**, **AF$_2$8/B** and **AF$_{23}$8/B**. Reagents and conditions: *i.* 1. $NaNO_2$, HCl, stirring 30 min. at −5 °C; 2. phenol, 2-fluorophenol, 3-fluorophenol or 2,3-difluorophenol, NaOH, dropwise addition over 30 min, stirring for 1 h; 3. $NaHCO_3$; *ii.* bromoalkane, $K_2CO_3$, KI, DMF, reflux, stirring, 18 h; *iii.* 7,7′-dibromoheptane, $K_2CO_3$, KI, acetone, reflux, stirring, 72 h; *iv.* 4-hydroxybenzaldehyde, $K_2CO_3$, KI, acetone, reflux, stirring, 72 h; *v.* $NaOCl_2$, $NaH_2PO_4$, resorcinol, tert-butanol, stirring at RT, overnight.

## 2. Materials and Methods

### *2.1. Characterization*

Thin-layer chromatography (TLC) was performed on an aluminum sheet precoated with silica gel. Analytical quality chemicals were obtained from commercial sources and used as obtained. The solvents were dried using the standard methods when required. The purity and the chemical structures of all synthesized materials were confirmed by the spectral data. The structure characterization of the prepared materials is based on $^1$H-NMR (Agilent Technologies 400 MHz VNMRS (Varian, Palo Alto, CA, USA) and Agilent Technologies 600 MHz shielded VNMRS (Varian, Palo Alto, CA, USA), in $CDCl_3$ solutions, with tetramethylsilane as an internal standard). Microanalyses were performed using a Leco CHNS-932 elemental analyzer (LECO Corporation, St. Joseph, MI, USA).

The mesophase behaviour and transition temperatures of the supramolecular complexes were measured using a Mettler FP-82 HT (Mettler-Toledo GmbH, Gießen, Germany) hot stage and control unit in conjunction with a Nikon Optiphot-2 polarizing microscope. The associated enthalpies were obtained from DSC thermograms, which were recorded on Perkin-Elmer DSC-8000 (PerkinElmer GmbH, Rodgau, Germany), with a heating and cooling rate of 10 K min$^{-1}$.

X-ray investigations were carried out with an Incoatec (Geesthacht, Germany) IμS microfocus source with a monochromator for CuK$\alpha$ radiation ($\lambda$ = 0.154 nm), and calibration was conducted with the powder pattern of $Pb(NO_3)_2$. A droplet of the sample was placed on a glass plate on the Linkam hot stage HFS-X350-GI (Linkam, Munich, Germany) (rate: 1 K min$^{-1}$–0.01 K min$^{-1}$). The exposure time was 5 min; the sample–detector distance was 9.00 cm for WAXS and 26.80 cm for SAXS. The diffraction patterns were recorded with a Vantec 500 area detector (Bruker AXS, Karlsruhe, Germany)and transformed into 1D plots using GADDS software (version number is 4.1.XX).

For the identification of hydrogen bond formation between the benzoic acid derivative **B** and the azopyridine components (**A**), FTIR measurements using the conventional KBr method and NMR analysis were conducted for some selected supramolecular complexes.

The photoisomerization studies in solution were conducted using an Ocean Optics HR 2000+ spectrophotometer, and absorption spectra were recorded at room temperature. The solutions in chloroform were taken in a 1 cm quartz cuvette and covered to avoid the evaporation of the solvent. The solutions were irradiated with UV light of 1 mW/cm$^2$ using Bluepoint LED Eco Hönle at a wavelength of 365 nm. A heat filter is inserted between the sample and the source to avoid the influence of UV heat on the sample. *Trans-cis*-trans photoisomerization in the LC phase was performed using 1 mW/cm$^2$ Bluepoint LED Eco Hönle at a wavelength of 365 nm.

### *2.2. Synthesis*

The synthesis of the hydrogen-bonded supramolecules (**A*n*/B**, **AF$_3$*n*/B**, **AF$_2$8/B**, and **AF$_{23}$8/B**) is shown in Scheme 1. The synthesis of the proton acceptors, i.e., the azopyridine derivatives (**A*n***, **AF$_3$*n***, **AF$_2$8**, and **AF$_{23}$8**) was performed using the same procedures described in our recent publication [36], starting with an azo coupling reaction between the diazonium salt of 4-aminopyridine (**1**) and phenol or different fluorinated phenols to give the corresponding azopyridine derivative **2**. Phenolic compound **2** was then etherified with different bromoalkanes via Williamson's reaction to yield the corresponding alkylated azopyridine derivatives (**A*n***, **AF$_3$8**, **AF$_2$8**, and **AF$_{23}$8**). As examples, the $^1$H NMR data of **A12**, **AF$_3$8**, **AF$_2$8,** and **AF$_{23}$8** are given below.

**4-(4-Decyloxyphenylazo)pyridine, A12.** Orange solid. 61% Yield, m.p. 73 °C. $^1$H NMR (400 MHz, $CDCl_3$) δ 8.77 (d, *J* = 6.0 Hz, 2H, Ar-H), 7.95 (d, *J* = 8.4 Hz, 2H, Ar-H), 7.71

(d, *J* = 6.0 Hz, 2H, Ar-H), 7.03 (d, *J* = 8.4 Hz, 2H, Ar-H), 4.06 (t, *J* = 6.4 Hz, 2H, Ar-O$\underline{CH_2}$), 1.85–1.76 (m, 2H, Ar-OCH$_2\underline{CH_2}$), 1.46–1.27 (m, 18H, $CH_2$), 0.90 (t, *J* = 6.8 Hz, 3H, -$CH_3$).

**4-(3-Fluoro-4-octyloxyphenylazo)pyridine, AF$_3$8**. Orange crystals. 30% Yield, m.p. 58–59 °C. $^1$H NMR (500 MHz, $CDCl_3$) δ 8.81–8.76 (m, 2H, Ar-H), 7.82 (ddd, *J* = 8.6, 2.3, 1.3 Hz, 1H, Ar-H), 7.72 (dd, *J* = 11.9, 2.3 Hz, 1H, Ar-H), 7.69–7.64 (m, 2H, Ar-H), 7.09 (t, *J* = 8.5 Hz, 1H, Ar-H), 4.14 (t, *J* = 6.6 Hz, 2H, Ar-OCH$_2$), 1.92–1.83 (m, 2H, Ar-OCH$_2\underline{CH_2}$), 1.55–1.29 (m, 10H, $CH_2$), 1.43–1.33 (m, 3H, -$CH_3$).

**4-(2-Fluoro-4-octyloxyphenylazo)pyridine, AF$_2$8**. Orange crystals. 37% Yield, m.p. 56–58 °C. $^1$H NMR (500 MHz, $CDCl_3$-*d*) δ 8.88–8.72 (m, 2H, Ar-H), 7.84–7.77 (m, 1H, Ar-H), 7.72–7.66 (m, 2H, Ar-H), 6.80–6.74 (m, 2H, Ar-H), 4.04 (t, *J* = 6.6 Hz, 2H, O-CH$_2$), 1.89–1.78 (m, 2H, Ar-O$\underline{CH_2}$), 1.52–1.42 (m, 2H, $CH_2$, Ar-OCH$_2\underline{CH_2}$), 1.42–1.23 (m, 8H, $CH_2$), 0.96–0.85 (t, *J* = 6.9 Hz, 3H, -$CH_3$).

**4-(2,3-Difluoro-4-octyloxyphenylazo)pyridine, AF$_{23}$8.** Orange crystals. 36.4% yield. m.p. 54–55 °C. **$^1$H NMR** (500 MHz, $CDCl_3$) δppm: 8.93–8.66 (m, 2H, Ar-H), 7.77–7.64 (m, 2H, Ar-H), 7.59 (ddd, *J* = 9.6, 7.5, 2.3 Hz, 1H, Ar-H), 6.82 (ddd, *J* = 9.4, 7.4, 2.0 Hz, 1H, Ar-H), 4.15 (t, *J* = 6.6 Hz, 2H, Ar-O$\underline{CH_2}$), 1.92–1.82 (m, 2H, Ar-OCH$_2\underline{CH_2}$), 1.55–1.44 (m, 2H, $CH_2$), 1.43–1.22 (m, 8H, $CH_2$), 0.96–0.80 (t, *J* = 6.8 Hz, 3H, -$CH_3$).

The synthesis of the proton donor (**B**) was performed as described in detail in our recent report [20]. Using Williamson's etherification reaction, 4-hydroxyphenyl-4-(dodecyloxy)benzoate (**3**) [42] was etherified with 7,7′-dibromoheptane to give intermediate compound **4**. An additional etherification step of **4** with 4-hydroxybenzaldehyde yielded aldehyde derivative **5**, which was then oxidized to the corresponding benzoic acid derivative **B** via Pinnick oxidation using sodium chlorite [20].

**B.** White crystals. Yield 97.7%, Cr 132 SmC 140 N 165 Iso. $^1$H NMR (600 MHz, $CDCl_3$) δ 9.88 (s, 1H, Ar-COOH), 8.19–8.08 (m, 2H, Ar-H), 8.08–8.00 (m, 2H, Ar-H), 7.14–7.04 (m, 2H, Ar-H), 6.98–6.85 (m, 6H, Ar-H), 4.04 (t, *J* = 6.5 Hz, 4H, Ar-O$\underline{CH_2}$), 3.97 (t, *J* = 6.5 Hz, 2H, Ar-O$\underline{CH_2}$), 1.95–1.70 (m, 6H, $CH_2$), 1.64–1.16 (m, 24H, $CH_2$), 0.97–0.79 (m, 3H, -$CH_3$).

### *2.3. Preparation of Supramolecular Complexes (**An/B**, **AF$_3$n/B**, **AF$_2$8/B**, **AF$_{23}$8/B**)*

The supramolecular complexes **A*n*/B**, **AF$_3$8/B**, **AF$_2$8/B**, and **AF$_{23}$8/B** were prepared by mixing equimolar amounts of each of the azopyridine derivatives **A*n***, **AF$_3$8**, **AF$_2$8**, and **AF$_{23}$8** with acid **B** in a DSC pan and melting them together with stirring until a homogeneous mixture was obtained. The mixture was cooled to room temperature, and the process was repeated twice to ensure hydrogen bond formation. As an example, the supramolecular complex **A8/B** was obtained by mixing **A8** (0.311 g, 1.0 mmol) with **B** (0.632 g, 1.0 mmol) as described above.

## 3. Results

### *3.1. Hydrogen Bond Formation*

To prove hydrogen bond formation between the proton donor and the proton acceptors, we performed FTIR as well as $^1$H NMR for selected representative examples. Figure 1a,b shows the FTIR spectra of the supramolecule **A12/B** (black curve) combined with the spectra of its individual components, i.e., acid **B** (blue curve) and nonfluorinated azopyridine **A12** (red curve) in two different regions (for the complete spectra, see Figure S1, Supplementary Materials). From Figure 1a, the FTIR bands of the supramolecule **A12/B** vary notably from those of the pure materials. For **A12/B,** two new broad bands at 2425 and 1885 cm$^{-1}$ appear due to the Fermi resonance overtones (also see Figure S1 in the Supplementary Materials) as typically observed for HBLCs [27,36]. More-

over, a shift to a higher wavenumber of the $\upsilon_{C=O}$ stretching vibration (1721, 1675 → 1721, 1684 $cm^{-1}$) for supramolecule **A12/B** compared to pure acid **B** can be observed (Figure 1b), indicating the successful formation of the hydrogen bond between **A12** and **B**. Similar results were observed for the fluorinated supramolecule **$AF_3$12/B** and its individual components **$AF_3$12** and **B** (see Figure S2a–c in the Supplementary Materials).

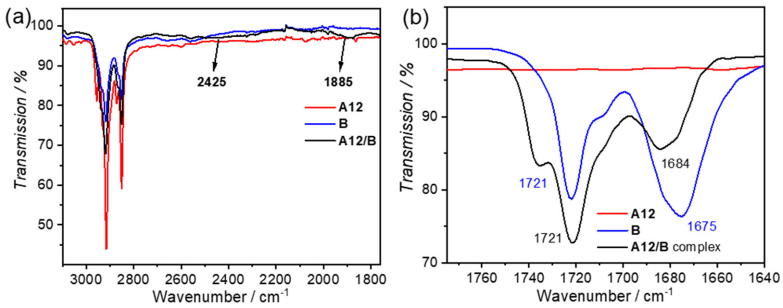


**Figure 1.** FTIR spectra of the supramolecule **A12/B** (black), benzoic acid derivative **B** (blue), and pure azopyridine compound **A12** (red) in a crystalline state at room temperature, and enlarged area (**a**) between 1750 $cm^{-1}$ and 3600 $cm^{-1}$ and (**b**) between 1620 $cm^{-1}$ and 1760 $cm^{-1}$ for the shift region of the C=O stretching vibration region.

Hydrogen bond formation was further confirmed by measuring the $^1$H NMR spectra for the pure materials before mixing them together and after the formation of the supramolecular hydrogen-bonded complex. As an example, the $^1$H NMR spectra of supramolecular **A12/B** (black), together with the spectra of pure benzoic acid derivative **B** (blue) and azopyridine derivative **A12** (red) in the aromatic region are shown in Figure 2 (for the complete spectra, see Figure S3). For the sake of comparison, the complete $^1$H NMR data for **A12**, **B**, and **A12/B** are given in the Supplementary Materials. Upon complexation, the signals of benzoic acid **B** in the aromatic region are slightly affected (compare the black and blue curves, Figure 2). Therefore, the chemical shifts of the multiplet signals recorded for pure **B** at 8.19–8.08 and 7.14–7.04 ppm are shifted to slightly lower δ values of 8.15–8.09 and 7.12–7.07 ppm, respectively. On the other hand, the change in the δ values after complexation is more obvious for **A12** in the aromatic region (compare the black and red curves, Figure 2). The recorded spectra of complex **A12/B** (black curve) reveal a higher chemical shift of all signals of the pyridine ring aromatic protons upon complex formation with acid **B**, where the doublet signals recorded for pure **A12** at 8.77, 7.95, 7.67 and 7.02 ppm are shifted to higher δ values upon complex formation as follows: 8.81, 7,97, 7.81, and 7.04, respectively. These observations, together with those from FTIR, confirm the successful formation of the hydrogen bond between complementary components **A12** and **B**.

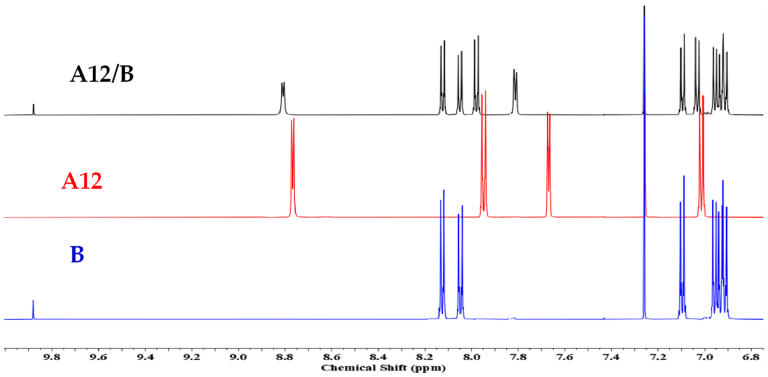


**Figure 2.** $^1$H-NMR spectra (500 MHz, $CDCl_3$) in the aromatic region of supramolecule **A12/B** (black) and the individual components, azo pyridine **A12** (red) and benzoic acid derivative **B** (blue). For the whole spectral range, see Figure S3 in the Supplementary Materials.

### 3.2. Mesomorphic Investigations

All the individual azopyridine derivatives used to construct the new supramolecules, i.e., **A*n*, AF$_3$8, AF$_2$8**, and **AF$_{23}$8,** are non-mesomorphic crystalline materials [16,36,43]. On the other hand, proton donor **B** is a liquid crystalline material exhibiting both nematic and smectic C phases with the following transition temperatures: Cr 132 °C SmC 140 °C N 165 °C Iso [20]. This LC behaviour of **B** is due to hydrogen bond formation between the free carboxylic groups, which results in the presence of **B** in a dimeric form. Upon mixing each of the azopyridine derivatives with proton donor **B,** different phase behaviour is observed. The transition temperatures (°C) and associated enthalpies (kJ mol$^{-1}$) as recorded by DSC measurements for all new supramolecular complexes are collected in Table 1 and shown graphically in Figure 3. As representative examples, the DSC thermograms recorded for supramolecular complexes **A12/B** and **AF$_3$12/B** are shown in Figure 4 (for all remaining DSC figures, see Figure S3 in the Supplementary Materials file). It should be noted that almost all supramolecules exhibit Cr-Cr transition during heating and cooling cycles (Figures 4 and S4). However, for clarity, we give in Table 1 the values of the peaks with higher values of transition enthalpy corresponding to the Cr-LC transition on heating or the LC-Cr transition on cooling cycles.

**Table 1.** Transition temperatures and enthalpies of the supramolecular complexes **A*n*/B**, **AF$_3$*n*/B**, **AF$_2$8/B**, and **AF$_{23}$8/B** [a].

| Complex | *n* | Phase Sequence (*T* [°C]/Δ*H* [kJ/mol]) |
|---|---|---|
| **A8/B** | 8 | **H**: Cr 115 [60.8] N 132 [5.1] Iso<br>**C**: Iso 130 [−5.0] N 98 [−60.4] Cr |
| **A10/B** | 10 | **H**: Cr 111 [41.1] N 128 [3.6] Iso<br>**C**: Iso 127 [−3.0] N 97 [−38.0] Cr |
| **A12/B** | 12 | **H**: Cr 117 [67.5] N 125 [3.0] Iso<br>**C**: Iso 123 [−4.0] N 101 [−66.4] Cr |
| **A14/B** | 14 | **H:** Cr 118 [89.5] N 126 [6.5] Iso<br>**C:** Iso 124 [−6.1] N 103 [−86.5] Cr |
| **AF$_3$8/B** | 8 | **H:** Cr1 104 [49.4] Cr2 110 [15.1] N 120 [3.3] Iso<br>**C:** Iso 119 [−2.4] N 92 [−55.6] Cr |
| **AF$_3$10/B** | 10 | **H:** Cr 105 [58.7] N 117 [5.5] Iso<br>**C:** Iso 117 [−2.6] N 100 [−0.5] M 93 [−58.2] Cr |
| **AF$_3$12/B** | 12 | **H:** Cr 107 [57.1] N 120 [3.2] Iso<br>**C:** Iso 118 [−3.0] N 100 [−61.8] Cr |
| **AF$_3$14/B** | 14 | **H:** Cr 107 [67.5] N 115 [2.2] Iso<br>**C:** Iso 114 [−2.4] N 98 [−67.2] Cr |
| **AF$_2$8/B** | 8 | **H:** Cr 96 [19.1] N 119 [1.2] Iso<br>**C:** Iso 119 [−1.2] N 88 [−20.8] Cr |
| **AF$_{23}$8/B** | 8 | **H:** Cr 94 [48.4] N 120 [4.2] Iso<br>**C:** Iso 118 [−3.5] N 85 [−46.0] Cr |

[a] Transition temperatures and enthalpy values were taken from the second DSC heating scans (10 K min$^{-1}$). Abbreviations: **H** = heating; **C** = cooling; Cr = crystalline state; N = nematic phase; M = unknown phase; Iso = isotropic liquid phase.

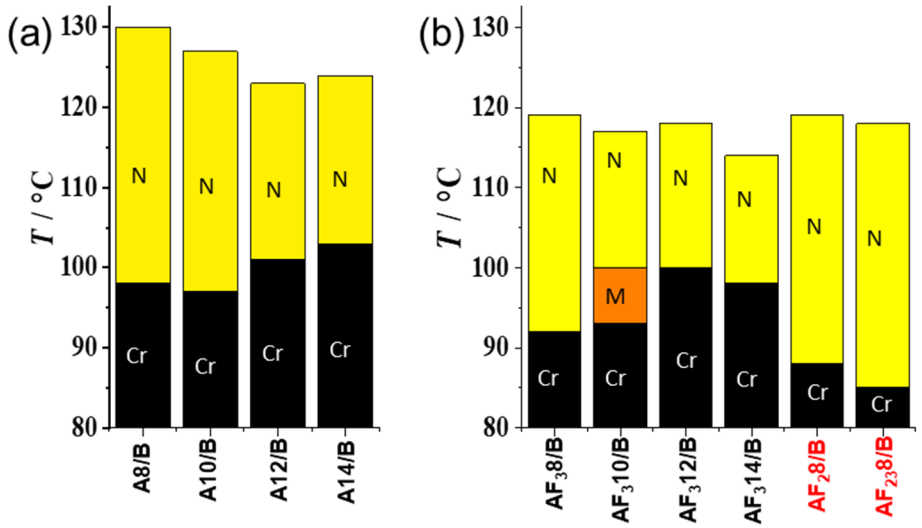


**Figure 3.** Bar diagram displaying LC-phases of the complexes **A*n*/B**, **AF$_3$*n*/B**, **AF$_2$8/B**, and **AF$_{23}$8/B** as determined from 2nd cooling DSC scans with a rate of 10 K min$^{-1}$. (**a**) Nonfluorinated HBLCs; (**b**) fluorinated HBLCs. Abbreviations: N = nematic phase (yellow); M = unknown phase (orange); Cr = crystalline solid (black). For numerical data and transition enthalpies, see Table 1.

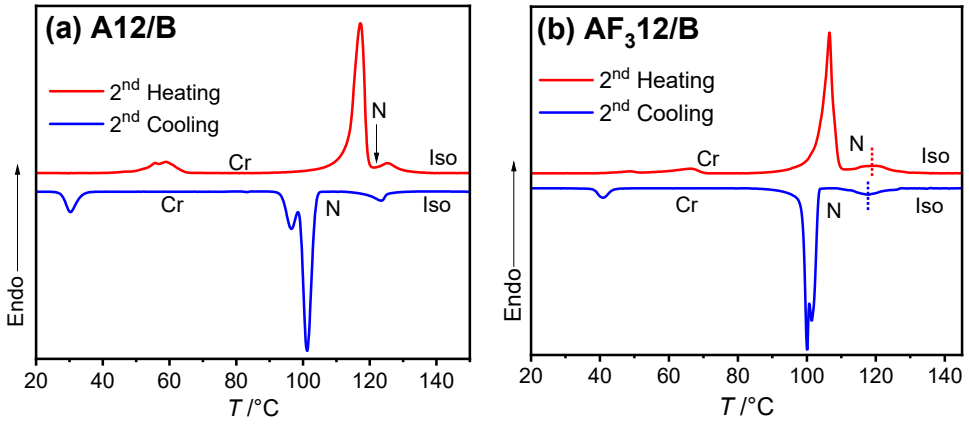


**Figure 4.** DSC thermograms recorded for the supramolecular complexes: (**a**) **A12/B** and (**b**) **AF$_3$12/B** with heating and cooling rates of 10 K/min.

### 3.2.1. Nonfluorinated HBLCs (**A*n*/B**)

As can be seen from Table 1 and Figure 3a, all the nonfluorinated supramolecules **A*n*/B** exhibit one type of an enantiotropic mesophase. As an example, on cooling supramolecule **A12/B** from the isotropic liquid state under POM, a schlieren texture could be observed (Figure 5a) as typically observed for nematic (N) phases. The transition from the crystalline state to the N phase on heating (N-Iso) or from Iso-N on cooling is associated with a measurable change in enthalpy, as measured during DSC investigations (Table 1 and Figure 4a). Similar DSC observations were also recorded for DSC thermograms of supramolecules **A*n*/B** (see Figure S4). The nematic phase was further confirmed by XRD investigations (see Section 3.3). The range of the nematic phase on heating is the same for the shorter supramolecules (**A8/B** and **A10/B**) of ~17 K on heating and ~30–32 K on cooling (Table 1 and Figure 4a). For the longer HBLCs (**A12/B** and **A14/B**), the nematic phase range is reduced (~8 K on heating and ~22 K on cooling).

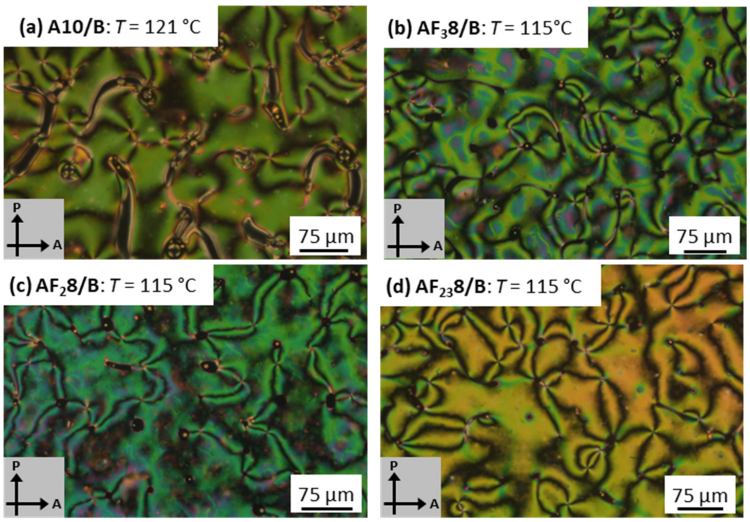


**Figure 5.** Optical textures of the nematic phase observed under crossed polarizers for the supramolecular complexes, (**a**) **A12/B**; (**b**) **AF$_3$8/B**; (**c**) **AF$_2$8/B,** and (**d**) **AF$_{23}$8/B** at the indicated temperatures on cooling from the isotropic state with 10 K/min.

### 3.2.2. Fluorinated HBLCs (**AF$_3$*n*/B**, **AF$_2$8/B**, **AF$_{23}$8/B**)

Mixing monofluorinated azopyridine derivatives **AF$_3$*n*** with acid **B** instead of the nonfluorinated analogues results in the fluorinated HBLCs **AF$_3$*n*/B**. The nematic phase is also the only observed LC on heating any of these supramolecules (Table 1 and Figure S4), which is also characterized by the Schlieren texture (Figure 5b). The nematic phase range for all fluorinated HBLCs with $n \leq 12$ is less compared to that of their related nonfluorinated HBLCs (**A*n*/B**, see Table 1 and Figure 3a,b). This could be attributed to an increased steric effect in the case of **AF$_3$*n*/B** supramolecules, resulting in lower phase stability. This effect has no significant role for the longest HBLCs, where the same nematic range is observed for both fluorinated and nonfluorinated HBLCs **A14/B** and **AF$_3$14/B** (~8 K on heating in both cases, Table 1).

An additional difference between **A*n*/B** and **AF$_3$*n*/B** could also be observed in the case of the supramolecule **AF$_3$10/B** with $n$ = 10. On cooling this HBLC under POM from the nematic phase, another LC phase with reduced birefringence could be observed (Figure 6b). This phase transition could also be detected during DSC investigations (see Table 1 and the DSC curve in Figure S4). This lower temperature phase is characterized by its higher viscosity compared to the N phase and its monotropic nature. Unfortunately, it was not possible to further characterize this metastable phase with XRD due to crystallization during the measurement time, and therefore, it is assigned as an M phase.

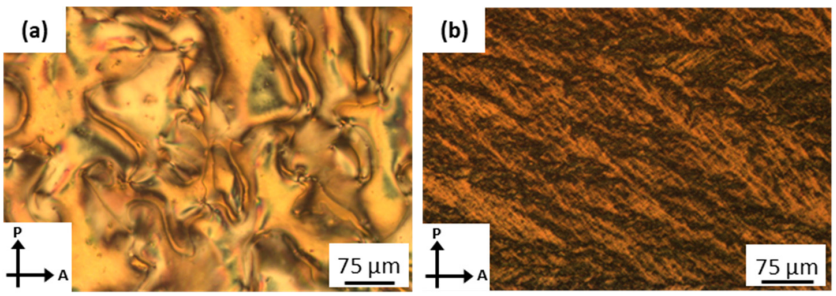


**Figure 6.** Optical textures between crossed polarizers for supramolecule **AF$_3$10/B**: (**a**) the nematic phase at $T$ = 108 °C and (**b**) M phase at $T$ = 98 °C on cooling from the isotropic state with 10 K/min.

Two additional selected examples of HBLCs with different positions and degrees of fluorine atoms were also constructed, namely **AF$_2$8/B** and **AF$_{23}$8/B**. In both cases, the

nematic phase was retained as the only observed mesophase, like their related analogues **A8/B** and **AF$_3$8/B** (see Figure 5c,d for the POM textures and Figure S4 for the DSC traces). However, the nematic phase range is increased for both **AF$_2$8/B** and **AF$_{23}$8/B** compared to **A8/B** and **AF$_3$8/B** (see Table 1 and Figure 3b). This could be a result of the change in the dipole moment because of the carbon–fluorine bonds resulting from using the F atom in an inner position in the case of **AF$_2$8/B** or by increasing the number of F atoms in the case of **AF$_{23}$8/B**. These structural modifications prove that aromatic core fluorination could be used successfully in these HBLCs to enhance the mesophase range.

### *3.3. XRD Investigations*

To further confirm the nature of the LC phases exhibited by the reported HBLCs, we conducted XRD experiments for two selected examples. For supramolecule **A12/B**, the SAXS region shows a broad peak at around $2\theta$ = 1.76° (5.03 nm) together with a broad wide-angle diffraction at $2\theta$ = 20.43° ($d_{WAXS}$ ~ 0.44 nm) (see Figure 7a) indicating the liquid-like state of the material and confirms the absence of fixed positions of molecules. Because of the maxima observed for the SAXS and WAXS signals, a spontaneous orientation of the nematic phase of **A12/B** can be assumed.

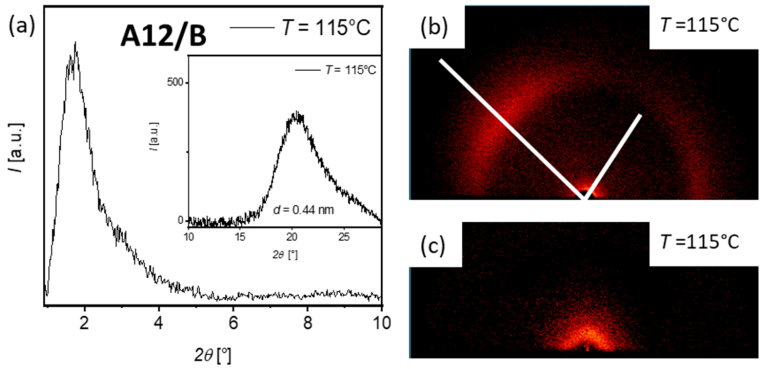


**Figure 7.** Measured XRD for supramolecule **A12/B** on cooling from isotropic liquid at $T$ = 115 °C: (**a**) 1D-XRD plot of the SAXS region, with inset showing WAXS region; 2D-XRD pattern for (**b**) WAXS region and (**c**) corresponding SAXS region.

For fluorinated supramolecular complex **AF$_3$12/B**, the nematic phase could also be confirmed by XRD experiments. Here, the SAXS region shows a broad peak at $2\theta$ = 1.65° (5.47 nm) with an additional WAXS halo at $2\theta$ = 20.65° ($d_{WAXS}$ = 0.44 nm) (see Figure 8a). The WAXS halo shows an equal distribution of signal intensity over the whole space, also confirming the presence of the nematic phase.

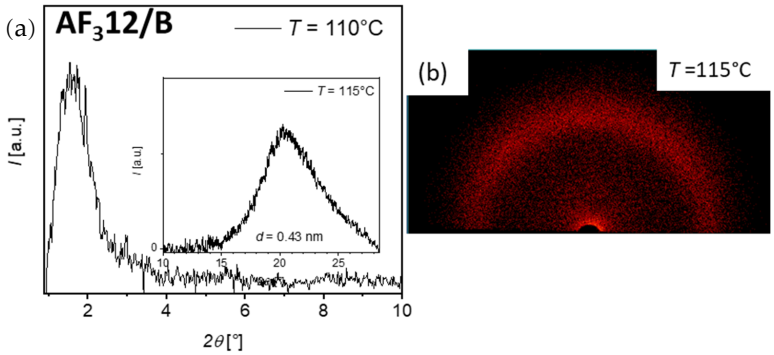


**Figure 8.** (**a**) 1D-XRD plots of compound **AF$_3$12/B** of the SAXS region, where the inset shows the WAXS region of the investigated supramolecular complex; the 2D-XRD pattern received for the WAXS region (**b**) measured on cooling from the isotropic liquid at $T$ = 115 °C.

### *3.4. Photoisomerization*

The incorporation of an azopyridine unit in the designed HBLCs enabled the investigation of *trans-cis* photoisomerization under light irradiation. As a representative example, Figure 9 illustrates the isothermal UV irradiation (365 nm) of supramolecular complex **A8/B** at 120 °C. Upon the irradiation of the nematic (N) phase, a rapid transition to the isotropic (Iso) phase occurs within three seconds (Figure 9a,b). When the light source is switched off, the system reverts to the N phase, confirming a fully reversible and fast photoswitching process between the Iso and N states. This behaviour arises from the *trans-cis* photoisomerization of the azopyridine unit, where the bent-shaped *cis*-isomer disrupts the molecular alignment, destabilizing the N phase and inducing the transition to isotropic. Such rapid and reversible phase transitions could be of interest for applications in optical data storage and nonlinear optical devices [44]. Similar photoswitching dynamics were observed for all N phases of other supramolecular complexes with the same alkyl chain length, regardless of the number or position of fluorine substituents (e.g., **AF$_3$8/B**, **AF$_2$8/B**, and **AF$_{23}$8/B**). This suggests that fluorination does not significantly influence the photoisomerization kinetics in these supramolecular dimers. For comparison, we also studied the photoisomerization of the HBLCs dissolved in chloroform using UV-Vis spectroscopy. However, the process was markedly very slow or even barely observed in solution (see Figure S5 for **A12/B** and **A12F$_3$/B**), highlighting the critical role of molecular packing and phase organization in photoswitching efficiency.

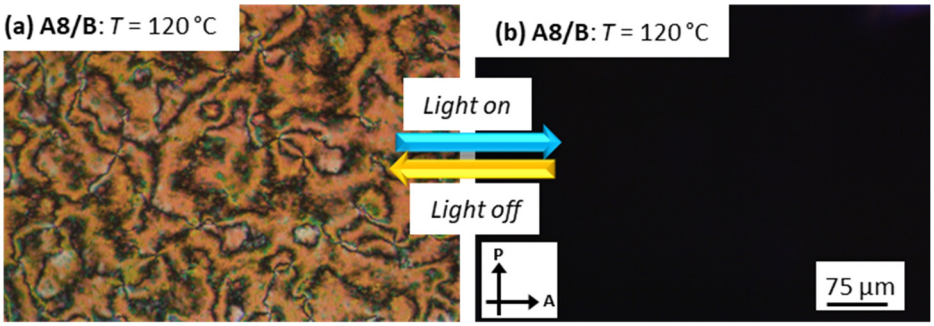


**Figure 9.** (**a**,**b**) Reversible photoisomerization for supramolecule **A8/B** between the nematic and isotropic liquid phases at 120 °C on cooling.

## 4. Conclusions

We successfully designed and prepared a new family of nonsymmetric supramolecular liquid crystalline dimers through intermolecular hydrogen bond formation. These supramolecules were formed between a benzoic acid derivative featuring a heptamethylene spacer (**B**) and various fluorinated and nonfluorinated azopyridine derivatives (**A*n*** and **A*n*F$_3$**). We also investigated the effect of changing the position of the fluorine atom or using double fluorination for selected examples on the phase behaviour of the supramolecules. The formation of a hydrogen bond between the complementary components was confirmed by FTIR and NMR experiments. All materials were investigated for their liquid crystalline behaviour using DSC, POM and XRD investigations. In all cases, the nematic phase was the only observed mesophase to be an enantiotropic one, which was further confirmed via XRD investigations. An additional unknown monotropic phase was observed only for **AF$_3$10/B** in a short range. Finally, we investigated the isothermal *trans-cis* photoisomerization of the reported supramolecules upon light irradiation, where a fast and reversible transition between the nematic and isotropic liquid phase was observed. These results highlight the importance of hydrogen bonding interaction in designing functional LC materials, avoiding multistep synthetic procedures.

**Supplementary Materials:** The following supporting information can be downloaded at: https://www.mdpi.com/article/10.3390/cryst15060576/s1, Figure S1: FTIR spectra of the supramolecule **A12/B** (black), benzoic acid derivative **B** (blue), and the pure azopyridine **A12** (red) in the crystalline state at room temperature. Figure S2a. FTIR spectra of the supramolecule **AF$_3$12/B** (black), benzoic acid derivative **B** (blue), and the pure azopyridine **AF$_3$12** (red) in the crystalline state at room temperature. Figure S2b. FTIR spectra of the supramolecule **AF$_3$12/B** (black) and its complementary components **AF$_3$12** (red) and **B** (blue): enlarged area between 1750 $cm^{-1}$ and 3600 $cm^{-1}$. Figure S2c. FTIR spectra of the supramolecule **AF$_3$12/B** (black) and its complementary components **AF$_3$12** (red) and **B** (blue): enlarged area between 1620 $cm^{-1}$ and 1760 $cm^{-1}$. Figure S3. $^1$H NMR spectra (500 MHz) of the supramolecule **A12/B** (black) and its complementary components, the azopyridine **A12** (red) and the benzoic acid derivative **B** (blue). Figure S4. DSC thermograms recorded for all supramolecular complexes reported in this study with heating and cooling rates of 10 $K/min^{-1}$. Figure S5. Spectral changes observed under UV light irradiation for: (a) **A12/B** and (b) **AF$_3$12/B** dissolved in chloroform.

**Author Contributions:** Conceptualization, writing—original draft preparation, writing—review and editing, supervision, funding acquisition, M.A.; methodology, validation, writing—original draft preparation, data curation, C.A. and M.A.; methodology, M.A.B. and T.N. All authors have read and agreed to the published version of the manuscript.

**Funding:** This research was funded by the German Research Foundation (DFG) (AL2378/1-2, 424355983, RTG 2670, 436494874).

**Data Availability Statement:** The original contributions presented in this study are included in the article/Supplementary Material, and further inquiries can be directed to the corresponding author.

**Conflicts of Interest:** The authors declare no conflicts of interest. The funders had no role in the design of the study; in the collection, analyses, or interpretation of data; in the writing of the manuscript; or in the decision to publish the results.

## References

1. Kato, T.; Uchida, J.; Ichikawa, T.; Sakamoto, T. Functional Liquid Crystals towards the Next Generation of Materials. *Angew. Chem.* **2018**, *57*, 4355–4371. [CrossRef] [PubMed]
2. Bisoyi, H.K.; Li, Q. Liquid Crystals: Versatile Self-Organized Smart Soft Materials. *Chem. Rev.* **2022**, *122*, 4887. [CrossRef]
3. Buchs, J.; Vogel, L.; Janietz, D.; Prehm, M.; Tschierske, C. Chirality Synchronization of Hydrogen-Bonded Complexes of Achiral N-Heterocycles. *Angew. Chem.* **2017**, *129*, 286–290. [CrossRef]
4. Kato, T.; Fréchet, J.M.J. A new approach to mesophase stabilization through hydrogen bonding molecular interactions in binary mixtures. *J. Am. Chem. Soc.* **1989**, *111*, 8533–8534. [CrossRef]
5. Wallage, M.J.; Imrie, C.T. Supramolecular dimeric liquid crystals. The liquid crystalline behaviour of mixtures of alpha-(4-pyridyloxy)-omega-4-(4-butylphenylazo)phenoxy alkanes and 4-octyloxybenzoic acid. *J. Mater. Chem.* **1997**, *7*, 1163–1167. [CrossRef]
6. Friot, B.; Boyd, D.; Willis, K.; Donnio, B.; Ungar, G.; Bruce, D.W. Hydrogen-bonded polycatenar mesogens. *Liq. Cryst.* **2000**, *27*, 605–611. [CrossRef]
7. Paleos, C.M.; Tsiourvas, D. Supramolecular hydrogen-bonded liquid crystals. *Liq. Cryst.* **2001**, *28*, 1127–1161. [CrossRef]
8. Kato, T.; Kamikawa, Y. *Handbook of Liquid Crystals*; Goodby, J.W., Collings, P.J., Kato, T., Tschierske, C., Gleeson, H., Raynes, P., Eds.; Wiley-VCH: Weinheim, Germany, 2014; Volume 5, pp. 513–540.
9. Alaasar, M.; Tschierske, C.; Prehm, M. Hydrogen-bonded supramolecular complexes formed between isophthalic acid and pyridine-based Derivatives. *Liq. Cryst.* **2011**, *38*, 925–934. [CrossRef]
10. de Oliveira, W.A.; Alaasar, M.; Cao, Y.; Westphal, E. 1,4-Bis(Acylhydrazone)-Based Polycatenar Liquid Crystals: Self-Assembly, Molecular Switching, and Gelation Properties. *ACS Omega* **2025**, *10*, 21637–21647. [CrossRef]
11. Jansze, S.M.; Martínez-Felipe, A.; Storey, J.; Marcelis, A.; Imrie, C.T. A Twist-Bend Nematic Phase Driven by Hydrogen Bonding. *Angew. Chem.* **2015**, *54*, 643–646. [CrossRef]
12. Walker, R.; Pociecha, D.; Abberley, J.P.; Martinez-Felipe, A.; Paterson, D.A.; Forsyth, E.; Lawrence, G.B.; Henderson, P.A.; Storey, J.M.D.; Gorecka, E.; et al. Hydrogen bonding and the design of twist-bend nematogens. *J. Mol. Liq.* **2020**, *303*, 112630. [CrossRef]
13. Walker, R.; Pociecha, D.; Martinez-Felipe, A.; Storey, J.M.D.; Gorecka, E.; Imrie, C.T. Twist-Bend Nematogenic Supramolecular Dimers and Trimers Formed by Hydrogen Bonding. *Crystals* **2020**, *10*, 175. [CrossRef]

14. Mandle, R. Supramolecular ferroelectric nematic materials. *Liq. Cryst.* **2022**, *49*, 2019–2026. [CrossRef]
15. Alaasar, M.; Poppe, S.; Dong, Q.; Liu, F.; Tschierske, C. Mirror symmetry breaking in cubic phases and isotropic liquids driven by hydrogen bonding. *Chem. Comm.* **2016**, *52*, 13869–13872. [CrossRef]
16. Alaasar, M.; Schmidt, J.-C.; Cai, X.; Liu, F.; Tschierske, C. Controlling liquid and liquid crystalline network formation by core-fluorination of hydrogen bonded supramolecular polycatenars. *J. Mol. Liq.* **2021**, *332*, 115870. [CrossRef]
17. Alaasar, M.; Cai, X.; Kraus, F.; Giese, M.; Liu, F.; Tschierske, C. Controlling ambidextrous mirror symmetry breaking in photosensitive supramolecular polycatenars by alkyl-chain engineering. *J. Mol. Liq.* **2022**, *351*, 118597. [CrossRef]
18. Imrie, C.T.; Henderson, P.A. Liquid crystal dimers and higher oligomers: Between monomers and polymers. *Chem. Soc. Rev.* **2007**, *36*, 2096–2124. [CrossRef]
19. Imrie, C.T.; Henderson, P.A.; Yeap, G.-Y. Liquid crystal oligomers: Going beyond dimers. *Liq. Cryst.* **2009**, *36*, 755–777. [CrossRef]
20. Cao, Y.; Zhao, Y.; Tan, T.; Liu, F.; Alaasar, M. Manipulation of Supramolecular Chirality in Bicontinuous Networks of Bent-Shaped Polycatenar Dimers. *Chem. Eur. J.* **2025**, *31*, e202403586. [CrossRef]
21. Zep, K.; Sitkowska, K.; Pociecha, D.; Górecka, E. Photoresponsive helical nanofilaments of B4 phase. *J. Mater. Chem. C* **2014**, *2*, 2323–2327. [CrossRef]
22. Bandarab, H.M.D.; Burdette, S.C. Photoisomerization in different classes of azobenzene. *Chem. Soc. Rev.* **2012**, *41*, 1809–1825. [CrossRef] [PubMed]
23. Alaasar, M. Azobenzene-containing bent-core liquid crystals: An overview. *Liq. Cryst.* **2016**, *43*, 2208–2243. [CrossRef]
24. Alaasar, M.; Prehm, M.; Nagaraj, M.; Vij, J.K.; Tschierske, C. A liquid crystalline phase with uniform tilt, local polar order and capability of symmetry breaking. *Adv. Mater.* **2013**, *25*, 2186–2191. [CrossRef]
25. Alaasar, M.; Poppe, S.; Dong, Q.; Liu, F.; Tschierske, C. Isothermal chirality switching in liquid-crystalline azobenzene compounds with non-polarized light. *Angew. Chem.* **2017**, *56*, 10801–10805. [CrossRef]
26. Paterson, D.A.; Xiang, J.; Singh, G.; Walker, R.; Agra-Kooijman, D.M.; Martinez-Felipe, A.; Gan, M.; Storey, J.M.D.; Kumar, S.; Lavrentovich, O.D.; et al. Reversible isothermal twist-bend nematic-nematic phase transition driven by the photoisomerization of an azobenzene-based nonsymmetric liquid crystal dimer. *J. Am. Chem. Soc.* **2016**, *138*, 5283–5289. [CrossRef]
27. Alaasar, M.; Schmidt, J.; Darweesh, A.F.; Tschierske, C. Azobenzene-based supramolecular liquid crystals: The role of core fluorination. *J. Mol. Liq.* **2020**, *310*, 113252. [CrossRef]
28. Blanke, M.; Balszuweit, J.; Saccone, M.; Wölper, C.; Jiménez, D.D.; Mezger, M.; Voskuhl, J.; Giese, M. Photo-switching and -cyclisation of hydrogen bonded liquid crystals based on resveratrol. *Chem. Commun.* **2020**, *56*, 1105–1108. [CrossRef]
29. Ren, H.; Yang, P.; Yu, H. Recent Progress in Azopyridine-Containing Supramolecular Assembly: From Photoresponsive Liquid Crystals to Light-Driven Devices. *Molecules* **2022**, *27*, 3977. [CrossRef] [PubMed]
30. Zaremba, M.; Siksnys, V. Molecular scissors under light control. *Proc. Natl. Acad. Sci. USA* **2010**, *107*, 1259–1260. [CrossRef]
31. Lee, K.M.; White, T.J. Photomechanical Response of Composite Structures Built from Azobenzene Liquid Crystal Polymer Networks. *Polymers* **2011**, *3*, 1447–1457. [CrossRef]
32. Garcia-Amorós, J.; Reig, M.; Castro, M.C.R.; Cuadrado, A.; Raposo, M.M.M.; Velasco, D. Molecular photo-oscillators based on highly accelerated heterocyclic azo dyes in nematic liquid crystals. *Chem. Comm.* **2014**, *50*, 6704–6706. [CrossRef] [PubMed]
33. Fehrentz, T.; Schönberger, M.; Trauner, D. Optochemical Genetics. *Angew. Chem.* **2011**, *50*, 12156–12182. [CrossRef] [PubMed]
34. Hird, M.; Goodby, J.W.; Lewis, R.A.; Toyne, K.J. The fascinating influence of fluoro substituents on the synthesis and properties of liquid crystals. *Mol. Cryst. Liq. Cryst.* **2003**, *401*, 1–18. [CrossRef]
35. Kirsch, P.; Bremer, M. Understanding Fluorine Effects in Liquid Crystals. *ChemPhysChem* **2010**, *11*, 357–360. [CrossRef]
36. Darweesh, A.F.; Anders, C.; Ranjitha, B.S.; Shanker, G.; Alaasar, M. On the impact of aromatic core fluorination in hydrogen-bonded liquid crystals. *RSC Adv.* **2025**, *15*, 6803–6816. [CrossRef] [PubMed]
37. Sergeyev, S.; Pisula, W.; Geerts, Y.H. Chem. Discotic liquid crystals: A new generation of organic semiconductors. *Soc. Rev.* **2007**, *36*, 1902–1929. [CrossRef]
38. Baghla, A.; Sahai, M.; Yadav, N.; Gupta, S.P.; Punjani, V.; Manjuladevi, V.; Vij, J.K.; Pal, S.K. Unusual polar ordering and room-temperature blue phase stabilization in tetrafluorinated bent-shaped mesogens. *Chem. Sci.* **2025**, *16*, 8002–8013. [CrossRef]
39. Zhang, W.; Peng, Z.; Pan, Q.; Liu, S.; Zhao, J. Effect of Fluorinated Substituents on Solubility and Dielectric Properties of the Liquid Crystalline Poly(ester imides). *ACS Appl. Polym. Mater.* **2022**, *5*, 141–151. [CrossRef]
40. Gibb, C.J.; Hobbs, J.; Nikolova, D.I.; Raistrick, T.; Berrow, S.R.; Mertelj, A.; Osterman, N.; Sebastián, N.; Gleeson, H.F.; Mandle, R.J. Spontaneous symmetry breaking in polar fluids. *Nat. Comm.* **2024**, *15*, 5845. [CrossRef]
41. Karcz, J.; Herman, J.; Rychłowicz, N.; Kula, P.; Gorecka, E.; Szydlowska, J.; Majewski, P.W.; Pociecha, D. Spontaneous chiral symmetry breaking in polar fluid–heliconical ferroelectric nematic phase. *Science* **2024**, *384*, 1096. [CrossRef]
42. Shivakumar, K.I.; Pociecha, D.; Szczytko, J.; Kapuściński, S.; Monobe, H.; Kaszyński, P. Photoconductive bent-core liquid crystalline radicals with a paramagnetic polar switchable phase. *J. Mater. Chem. C* **2020**, *8*, 1083–1088. [CrossRef]

43. Alaasar, M.; Tschierske, C. Nematic phases driven by hydrogen-bonding in liquid crystalline nonsymmetric dimers. *Liq. Cryst.* **2019**, *46*, 124–130. [CrossRef]
44. Alaasar, M.; Nirgude, T.; Anders, C. The influence of bromine substitution and linking groups on the phase behaviour of light-responsive rod-like molecules. *J. Mol. Liq.* **2024**, *414*, 126174. [CrossRef]